Results in Physics 19 (2020) 103488

Contents lists available at ScienceDirect

Results in Physics

journal homepage: www.elsevier.com/locate/rinp

Structural and shielding properties of NiO/xCo_3O_4 nanocomposites synthesized by microwave irradiation method

Atif Mossad Ali [a], Shams A.M. Issa [b,c], Hesham M.H. Zakaly [c,d], Mariia Pyshkina [d,e], H. H. Somaily [a], H. Algarni [a], M. Rashad [b,f], M. Saif [d], H.A.A. Sidek [g], K.A. Matori [g], M.H.M. Zaid [g,*]

[a] Physics Department, Faculty of Science, King Khalid University, Abha, Saudi Arabia
[b] Department of Physics and Nanotechnology Research Unit, Faculty of Science, University of Tabuk, Tabuk, Saudi Arabia
[c] Physics Department, Faculty of Science, Al-Azhar University, Assiut 71524, Egypt
[d] Institute of Physics and Technology, Ural Federal University, Yekaterinburg, Russia
[e] Institute of Industrial Ecology UB RAS, Ekaterinburg, Russia
[f] Physics Department, Faculty of Science, Assiut University, Assiut 71516, Egypt
[g] Department of Physics, Universiti Putra Malaysia, 43400 Serdang, Selangor, Malaysia

ARTICLE INFO

Keywords:
NiO/Co_3O_4
Nanoparticles
Structure
Shielding properties

ABSTRACT

In the present study, nanocomposites with different ratios of NiO and Co_3O_4 (x = 0.3, 0.5, and 0.7) have been prepared via microwave oven and characterized using XRD. FLUKA code has been used to estimate the values of the mass attenuation coefficient (μ_m) for all samples. From the measurement, we found that when the thickness of the samples increases, the gamma transmission values decrease. Besides, the μ_m values increase as the Co_3O_4 content increase from 0.3 to 0.7%. At selected photon energy, the HVL, TVL, and MFP values decrease with increasing Co_3O_4 concentrations. At low energies (0.1–0.5 MeV), the linear decreasing trend in MAC values indication that photoelectric effect (PEA) ($\propto 1/E^{3.5}$) dominance over this region. Afterward, at medium energy regions (0.5–1.33 MeV), the decrements in MAC values are insignificant as the Compton scattering (CS) ($\propto 1/E$) phenomenon dominates. As a conclusion, CoNi3 has superior effectiveness as a shielding material.

Introduction

Nanotechnology develops a new branch for improving the properties of materials. In past days the investigation of nanoparticles has been performed by different researchers [1]. The growth of transition metal investigations such as tricobalt tetraoxide and NiO which are interesting and favorable transition oxide due to their importance in many implementations like a store of data, gas detecting, catalysts, and electrochemical instruments [1–3]. Though improvement of technology has made human being life easier, this improvement has disadvantages like quick development of utilizing radioactive sources in our daily life including manufactures, medicinal diagnostic facilities, reactors, radiation waste store places, radiation study institutes, the nourishment sterilization, and medicinal therapy [4–6]. Nanocomposites materials have been studied by many researchers, Jabeen et al. were recorded that the $(In_2O_3)_{30}/(NiO)_{70}$ nanocomposite sample is an appropriate nominee for electrode material in electrochemical application [7]. Gupta and Ahmed studied the structure, magnetic, and optical properties of Co_3O_4-NiO nanocomposites samples [8]. The Electrochemical, mechanical and adhesive properties of surface-modified NiO-epoxy nanocomposite coatings on mild steel have been done by Xavier [9]. Alghazzawi et al. used the microwave hydrothermal method for the synthesis of rGO/NiO nanocomposite samples. They also recorded that the rGO/NiO nanocomposite is used as a sensitive nonenzymatic glucose sensor [10].

Due to the mischievous influences of ionizing radiation, the safeguard of humans against radiation has become a stringent problem. Thus, providing a suitable protective material is permanently very important in the radiation safety field [11]. Among all kinds of radiation, protection against gamma has become large attention because of their extremely penetration nature. Despite the high competence of traditional Pb and concrete in attenuate gamma, they have some disadvantages [12]. For example, it is hard to be confirmed of concretes efficiency in radiation shielding due to their moisture changing and nonhomogeneity. Also, the poisonous nature of Pb has been performed in being deserted by numerous industries [13].

The protection strength of the shield depends on three parameters;

* Corresponding author.
E-mail address: drhafizzaid2020@gmail.com (M.H.M. Zaid).

https://doi.org/10.1016/j.rinp.2020.103488
Received 8 August 2020; Received in revised form 17 September 2020; Accepted 6 October 2020
Available online 12 October 2020

radiation energy, the absorbent density, and Z in the shield [14,15]. Thus, there are two ways to progress the protection features of the shield: appropriate elements and the decrease of material pores [16]. Nanomaterials are excessively utilized in different applications. A nanoparticle is a very tiny particle generally with a size < 100 nm, that could be utilized in materials. Nanomaterials are very attractive because of the very tiny size and high particular surface area and have a high possibility for beneficent material features like compressive strength and permeability [17]. In this regard, the nanoparticle performs some special tasks as a radiation shield; it could be reducing gamma. Besides, its properties can be easily changed by changing its composition. The study of gamma radiation shielding for NiO/xCo_3O_4 nanocomposites prepared samples is novel because there is no such study in the literature. In addition, the novelty of this study is the use of the FLUKA Monte Carlo code to evaluate the mass attenuation coefficient for NiO/xCo_3O_4 nanocomposites samples in the photon energy range from 0.1 to 1.33 MeV.

Experimental techniques

The samples were prepared using a microwave oven (650 W) [18]. The starting materials are cobalt nitrate hexahydrate and nickel nitrate hexahydrate were used. The purity of these materials is equal to 97%. For pure Co_3O_4 and, NiO, for example (Co_3O_4 NPs), it was fabricated by adding twenty-five (ml) H_2O solution of 0.2 mol. cobalt nitrate hexahydrate, with a 25 ml H_2O solution containing 0.2 mol in a flask. The same procedures were used for the preparation NiO NPs using the starting material of Nickle nitrate hexahydrate. The solution was put in a microwave furnace operating at a maximum of 20 min.

The fine powder of Co_3O_4 and NiO-NPs is collected for descriptions. For mixed nanocomposites of NiO/Co_3O_4 were fabricated via the same process. Various contents of (30, 50, and 70 wt%) of cobalt nitrate hexahydrate are mixed with (70, 50 and 30 wt%) of nickel(II) nitrate hexahydrate with 0.2 mol. A fine powder of (NiO/Co_3O_4) nanocomposites is taken away. The samples (1-*x*)NiO/*x*Co_3O_4 with $x = 30$, 50, and 70 wt% are called CONi1, CONi2, and CONi3, respectively. This method for preparing nanoparticle is considered as a promising technique due to the easy and sheep aspects. Moreover, the smallest preparation time is one of the most features. The prepared samples are fine powder possessing uniform particle size. XRD measurements were carried via a Shimadzu XD-3A X-ray diffractometer CuKα radiations (λ = 0.15418 nm).

FLUKA is a radiation transport code based on the Monte Carlo method. FLUKA code [19–21] was developed collaboratively by CERN and INFN, can be found elsewhere (Fig. 1) [22–24]. FLUKA code was utilized to evaluate the shielding features of three samples of (1-x)NiO/xCo_3O_4, where (x = 0.3, 0.5, and 0.7) nanocomposites against γ-rays. In the present simulation, The BEAMPOS card was used to define the position and direction of the radioactive source which is considered as a monoenergetic (0.2 cm dimension), a mono-directional beam of photons along plus z-axis with different energies at 15–15 × 10^3 KeV. Then the angular and energy distribution of the source and the type of particle and its energy was known by the BEAM card. For photon transport at low energies, the energy cut-off is 10^{-6} GeV by EMFCUT card. The photons were detecting via NaI (Tl) (7.62 × 7.62 cm) scintillation detector. The detector was placed inside the lead cylinder collimator has a 120 and 2 mm outer and inner diameter, respectively with a 130 mm height. The NaI area was realized as the track-length fluence evaluator via the USRTRACK scorecard. In geometry, the sample was located between the source, and the detector surface is indicated in Fig. 1.

MATERIAL card describing the chosen sample contains the mixture name, weight fraction, specimen number, and density, etc. and it's used with wanted COMPOUND cards to determine the exact composition of the sample. Simulation processes run between 10^6 and 20^6 number of primary photons to obtain a statistical error <1%. The fluence of a photon in the volume of a detector was assessed with the USRBIN card. The sample was modeled as a cylinder, 40 mm diameter, with the different thicknesses from 2 to 5 mm. Glass samples were conducted with the Rectangular Parallelepiped body. RPP is characterized by 6 numbers X (min and max), Y (min and max), Z (min and max) and has edges parallel to the coordinate axes. In this simulation geometry, X (min and max), and Y (min and max) were chosen as −50 and +50 mm, respectively. Photons passing through the sample have been detected in detector volume.

Results and discussion

XRD measurements

Fig. 2 shows the XRD diffraction pattern of different compositions of (1-*x*)NiO/*x*Co_3O_4 NPs of (30, 50, and 70 wt%). As shown in Fig. 2, the 0.7NiO/0.3Co_3O_4 NPs nanocomposites show eight peaks, which indicated to NiO NPs [25,26] with 3 additional three peaks at the angle of 44, 52, and 76°. These three peaks are related to 30 wt% Co_3O_4 NPs. With increasing Co_3O_4 NPs content 0.5NiO/0.5Co_3O_4 NPs, the intensity of these 3 peaks enhanced as illustrated in Fig. 2. For the 0.3NiO/0.7Co_3O_4 NPs as shown in Fig. 2, these distinguish peaks are shifted to angles of 32, 59, and 65°. This indicates a new phase of the p-p nanocomposite. The crystalline size of the NiO/Co_3O_4 NPs with different concentrations of (30, 50, and 70 wt%) could be calculated using the following expression [27]:

$$D = \frac{0.94\lambda}{\beta cos\theta} \quad (1)$$

where, λ and β are the wavelength and FWHM of the diffraction peak,

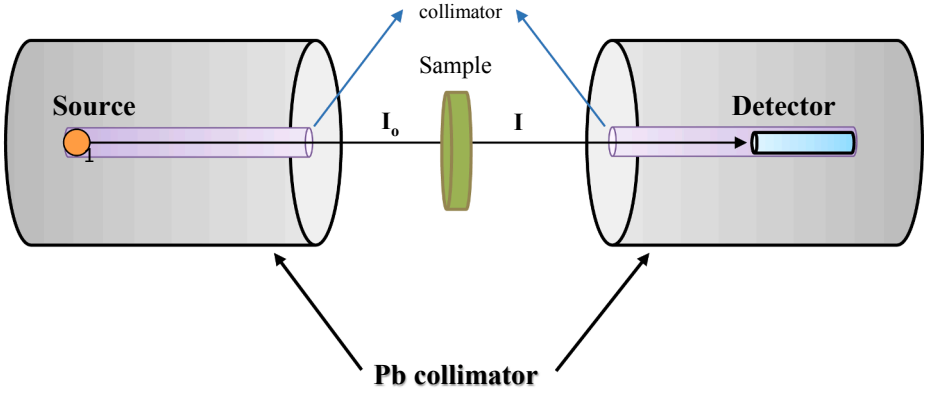

Fig. 1. FLUKA Monte Carlo simulation setup used for mass attenuation coefficients calculations of glasses.

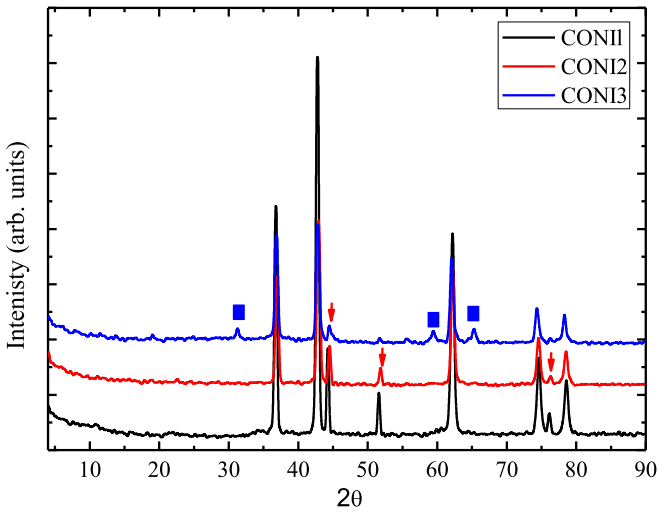

Fig. 2. XRD pattern of (100-x)NiO/xCo_3O_4 composites.

respectively. The evaluated values of crystalline size are in the range of fourteen nm. The ionic radius of the host material of Ni^{2+} is 69 pm [28]. On the other hand, the Co^{2+} ionic radius is 65 pm [29]. Substitution alloys are expected because of that the host and foreign material are nearly similar.

Shielding parameters

If the radiation source is positioned between the counter detector and the absorber it decreases exponentially due to Beer-Lambert law and gamma rays that pass through the attenuator [30–32]:

$$I = I_o e^{-\mu x} \tag{2}$$

where I_o is the intensity of non-attenuated and I, is the intensity of attenuated gamma during the specimen. Also, μ represents the linear attenuation coefficient and *x*iis the specimen thickness. In the case of a compound, the mass attenuation coefficients (μ_m) are evaluated via the compound rule.

$$\mu_m = \sum_i w_i (MAC)_i \tag{2}$$

where w_i is the weight fraction of the i^{th} constitute elements. The desired sample thickness should reduce the absorbed gamma to one-half are called the half-value layer (HVL), and are acquired using the following equations [33–35]:

$$HVL = \frac{\ln(2)}{LAC} \tag{3}$$

Samples with a thickness of one mean free path (MFP) absorb 0.368 of the initial gamma intensity when it passes through the samples. It is calculated by [31,36,37]:

$$MFP = \frac{1}{LAC} \tag{4}$$

Gamma transmission (T) of the studied samples was evaluated for 356, 662, 1173, and 1332 keV. The changes of evaluated T were presented against sample thickness (*x*) in Fig. 3 for the CONi2 sample (an example). When *x* of the samples increases, the T values reduce quickly and increase as the photon energy increase. Fig. 4 shows the T values against sample thickness for all studied samples. As shown in this figure, the CONi3 sample has the lowest T among the studied samples. It is also evident from Figs. 3 and 4 the x-dependent vary of the Ts moves away from linearity with increment energy. This indicates that for high energy the specimen thickness must be increased. For all CONi1, CONi2, and

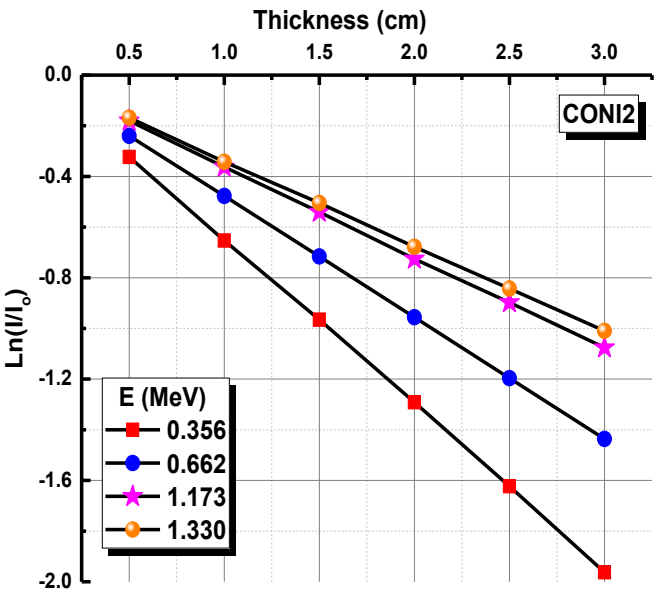

Fig. 3. Variation of transmission photon flux as a function of CONI2 sample thicknesses.

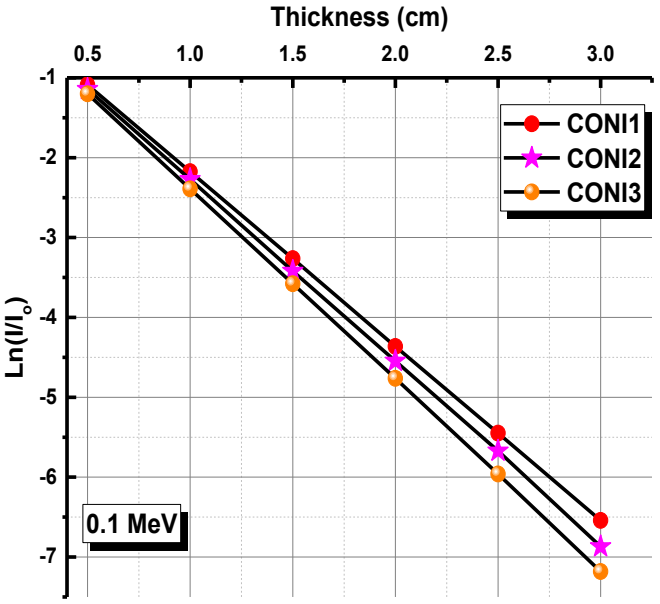

Fig. 4. Variation of transmission photon flux as a function of samples thicknesses at 0.1 MeV.

CONi3 samples Fig. 5 illustrates the changes in MAC, derived by applying FLUKA code at 0.1–1.33 MeV. It can be seen from Fig. 5 that with γ-ray energy increment from 0.1 to 1.33 MeV, from CONi1 to CONi3 samples, MAC values follow the same trend and improved noticeably with growing Co_3O_4 compound. Sample CONi3 possesses comparatively greater MAC values owing to bigger wt. % of Co_3O_4 in it, in all investigated glasses. For instance, at 0.1 MeV, 0.3472, 0.3567, 0.3673 (cm^2/g) are the calculated MAC values for CONi1, CONi2, and CONi3 specimens, respectively. At low energies (0.1–0.5 MeV), for CONi1, CONi2, and CONi3 specimens, the noticed speedy reduction in MAC values indication that photoelectric effect (PEA) ($\propto 1/E^{3.5}$) dominance over this region. Afterward, at medium energy regions (0.5–1.33 MeV), the decrements in MAC values are insignificant as the Compton scattering (CS) ($\propto 1/E$) phenomenon dominates [38,39].

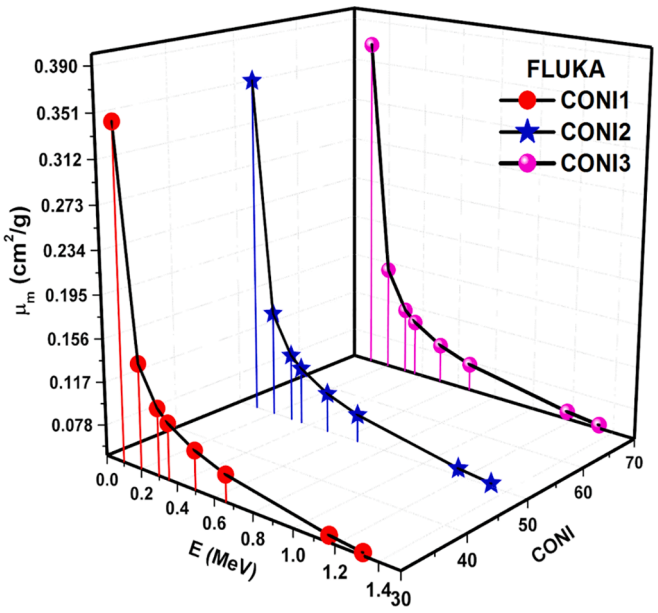

Fig. 5. Mass attenuation coefficient (μ_m) values for investigated samples against photon energy.

HVL, TVL, and MFP are indispensable parameters in assessing a material's gamma shielding competence, and commonly, the lower these values, the higher the shielding performance concerning sample thickness requirements. It is well known that lower HVL, TVL, and MFP refer to excellent protection capacity [20–24,33]. These factors with the same behavior of change against photon energy and sample compositions are given in Figs. 6–8, respectively. The calculated HVL, TVL, and MFP values change for CONi1, CONi2, and CONi3 samples within 356–1332 keV. Following Figs. 6–8, one can observe that for all investigated samples measured HVL, TVL, and MFP values show the same variance with photon energy. It is obvious that to decrease incident lower energy a very less glass thickness is enough. Then, with increasing photon energy, HVL, and MFP increase faster, approaching the corresponding largest values, indicating a bigger sample thickness requisite to reduce incoming gamma energy. As explained before, for μ_m behaviors, The HVL, TVL, and MFP values depend on the incident photon energy corresponding to CS mechanisms dominates at medium energy.

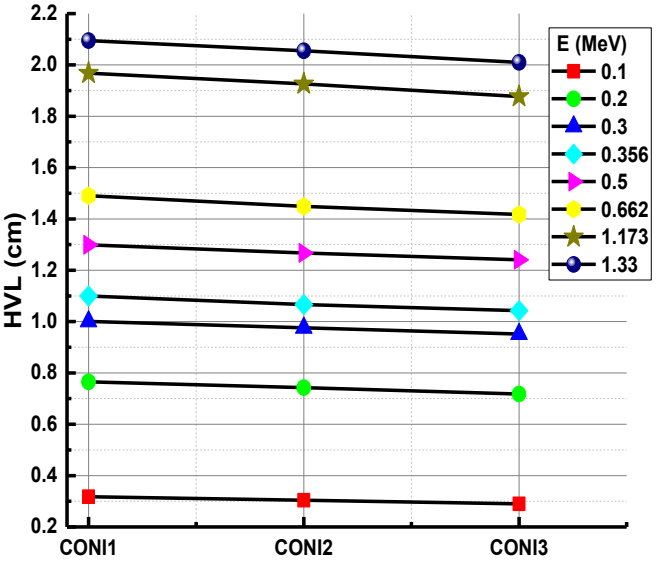

Fig. 6. Variation of HVL for investigated samples.

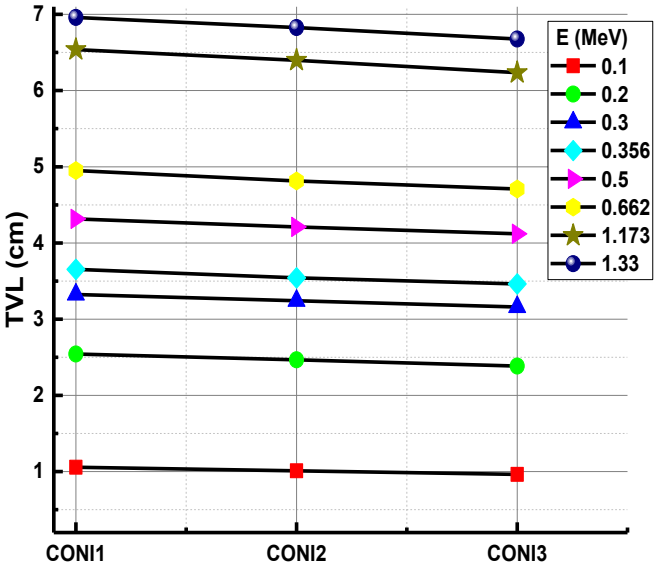

Fig. 7. Variation of TVL for investigated samples.

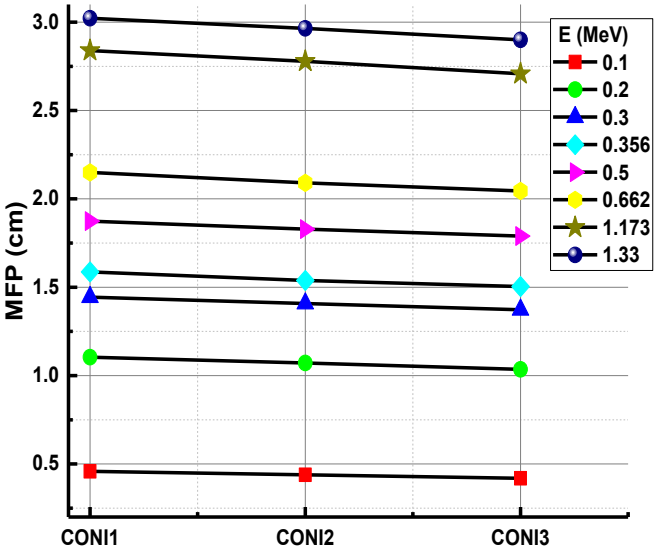

Fig. 8. Variation of MFP for investigated samples.

Furthermore, Figs. 6–8 show that HVL, TVL, and MFP values gradually decrease with increasing NiO concentration for CONi1, CONi2, and CONi3 samples. In all investigated samples, the relatively minimal thickness is required for sample CONi3 when compared to the rest of the samples to absorb photons as density improves for CONi1, CONi2, and CONi3 samples

Conclusion

The (1-*x*)NiO/*x*Co_3O_4 NPs of (30, 50 and 70 wt%). NPs were synthesized via the microwave irradiation method. These samples were checked using experimental XRD data. These obtained results confirmed the nature phase of the (1-*x*)NiO/*x*Co_3O_4 nanocomposites. The sizes of these NPs were found to be in the range of 14 nm. Moreover, the addition of Co_3O_4 improves the radiation shielding properties of (1-*x*)NiO/*x*Co_3O_4 nanocomposites samples.

CRediT authorship contribution statement

Atif Mossad Ali: Conceptualization, Methodology, Investigation, Writing - original draft. **Shams A.M. Issa:** Writing - original draft, Funding acquisition, Supervision. **Hesham M.H. Zakaly:** Writing - original draft, Supervision. **Mariia Pyshkina:** Conceptualization. **H.H. Somaily:** Investigation. **H. Algarni:** Conceptualization. **M. Rashad:** Conceptualization, Methodology. **M. Saif:** Conceptualization. **H.A.A. Sidek:** Conceptualization, Methodology. **K.A. Matori:** Conceptualization, Methodology. **M.H.M. Zaid:** Writing - original draft, Funding acquisition, Supervision.

Declaration of Competing Interest

The authors declare that they have no known competing financial interests or personal relationships that could have appeared to influence the work reported in this paper.

Acknowledgments

The authors express their gratitude to the Deanship of Scientific Research at King Khalid University for funding this work through research groups program under grant number R.G.P. 2/33/41 and Universiti Putra Malaysia for the research and publication funding.

References

[1] Shahid MM, Rameshkumar P, Huang NM. Morphology dependent electrocatalytic properties of hydrothermally synthesized cobalt oxide nanostructures. Ceram Int 2015;41:13210–7. https://doi.org/10.1016/j.ceramint.2015.07.098.
[2] Bartůněk V, Huber Š, Sedmidubský D, Sofer Z, Šimek P, Jankovský O. CoO and Co3O4 nanoparticles with a tunable particle size. Ceram Int 2014;40:12591–5. https://doi.org/10.1016/j.ceramint.2014.04.082.
[3] Rashad M, Darwish AAA, AlGarni SE. High electrical conductivity of (1-x)NiO/xFe2O3(x = 0.0, 0.3, 0.5, 0.7 and 1) nanoparticles for solid-state electronics. J Magn Magn Mater 2019;491:165577. doi:10.1016/j.jmmm.2019.165577.
[4] Almeida Junior TA, Nogueira MS, Vivolo V, Potiens MPA, Campos LL. Mass attenuation coefficients of X-rays in different barite concrete used in radiation protection as shielding against ionizing radiation. Radiat Phys Chem 2017;140:349–54. https://doi.org/10.1016/j.radphyschem.2017.02.054.
[5] Singh H, Singh K, Gerward L, Singh K, Sahota HS, Nathuram R. ZnO–PbO–B2O3 glasses as gamma-ray shielding materials. Nucl Instrum Methods Phys Res Sect B 2003;207:257–62. https://doi.org/10.1016/S0168-583X(03)00462-2.
[6] More CV, Alavian H, Pawar PP. Evaluation of gamma-ray attenuation characteristics of some thermoplastic polymers: Experimental, WinXCom and MCNPX studies. J Non Cryst Solids 2020;546:120277. doi:10.1016/j.jnoncrysol.2020.120277.
[7] Jabeen S, Iqbal J, Arshad A, Williams J, Samarin S, Rani M. Heterojunction formation in In_2O_3–NiO nanocomposites: towards high specific capacitance. J Alloys Compd 2020;842:155840. https://doi.org/10.1016/j.jallcom.2020.155840.
[8] Gupta J, Ahmed AS. Interfacial exchange coupling and defects driven magnetic and optical properties of Co3O4-NiO nanocomposites. Phys B Condens Matter 2020:412383. https://doi.org/10.1016/j.physb.2020.412383.
[9] Xavier JR. Electrochemical, mechanical and adhesive properties of surface modified NiO-epoxy nanocomposite coatings on mild steel. Mater Sci Eng B 2020;260:114639. https://doi.org/10.1016/j.mseb.2020.114639.
[10] Alghazzawi W, Danish E, Alnahdi H, Salam MA. Rapid microwave-assisted hydrothermal green synthesis of rGO/NiO nanocomposite for glucose detection in diabetes. Synth Met 2020;267:116401. https://doi.org/10.1016/j.synthmet.2020.116401.
[11] Kumar A. Gamma ray shielding properties of PbO-Li2O-B2O3 glasses. Radiat Phys Chem 2017;136:50–3.
[12] Issa SAM, Ahmad M, Tekin HO, Saddeek YB, Sayyed MI. Effect of Bi2O3 content on mechanical and nuclear radiation shielding properties of Bi_2O_3-MoO_3-B_2O_3-SiO_2-Na_2O-Fe_2O_3 glass system. Results Phys 2019;13:102165. https://doi.org/10.1016/j.rinp.2019.102165.
[13] Uosif MAM, Mostafa AMA, Issa SAM, Tekin HO, Alrowaili ZA, Kilicoglu O. Structural, mechanical and radiation shielding properties of newly developed tungsten lithium borate glasses: an experimental study. J Non Cryst Solids 2020;532:119882. https://doi.org/10.1016/j.jnoncrysol.2019.119882.
[14] Hassan HE, Badran HM, Aydarous A, Sharshar T. Studying the effect of nano lead compounds additives on the concrete shielding properties for γ-rays. Nucl Instrum Methods Phys Res Sect B 2015;360:81–9. https://doi.org/10.1016/j.nimb.2015.07.126.
[15] Nikbin IM, Shad M, Jafarzadeh GA, Dezhampanah S. An experimental investigation on combined effects of nano-WO3 and nano-Bi2O3 on the radiation shielding properties of magnetite concretes. Prog Nucl Energy 2019;117:103103. https://doi.org/10.1016/j.pnucene.2019.103103.
[16] Gencel O, Bozkurt A, Kam E, Korkut T. Determination and calculation of gamma and neutron shielding characteristics of concretes containing different hematite proportions. Ann Nucl Energy 2011. https://doi.org/10.1016/j.anucene.2011.08.010.
[17] Ozyildirim C, Zegetosky C. Exploratory investigation of nanomaterials to improve strength and permeability of concrete. Transp Res Rec J Transp Res Board 2010;2142:1–8. https://doi.org/10.3141/2142-01.
[18] Sheikholeslami M, Rokni HB. Melting heat transfer influence on nanofluid flow inside a cavity in existence of magnetic field. Int J Heat Mass Transf 2017;114:517–26. https://doi.org/10.1016/j.ijheatmasstransfer.2017.06.092.
[19] Zakaly HM, Abouhaswa AS, Issa SAM, Mostafa MYA, Pyshkina M, El-Mallawany R. Optical and nuclear radiation shielding properties of zinc borate glasses doped with lanthanum oxide. J Non Cryst Solids 2020;543:120151. https://doi.org/10.1016/j.jnoncrysol.2020.120151.
[20] Rashad M, Tekin HO, Zakaly HM, Pyshkina M, Issa SAM, Susoy G. Physical and nuclear shielding properties of newly synthesized magnesium oxide and zinc oxide nanoparticles. Nucl Eng Technol 2020. https://doi.org/10.1016/j.net.2020.02.013.
[21] Elazaka AI, Zakaly HMH, Issa SAM, Rashad M, Tekin HO, Saudi HA, et al. New approach to removal of hazardous Bypass Cement Dust (BCD) from the environment: 20Na2O-20BaCl2-(60–x)B2O3-(x)BCD glass system and Optical, mechanical, structural and nuclear radiation shielding competences. J Hazard Mater 2020;403:123738. https://doi.org/10.1016/j.jhazmat.2020.123738.
[22] Ferrari A, Sala PR, Fasso A, Ranft J. FLUKA: a multi-particle transport code. CERN-2005-10 2005:INFN/TC 05/11, SLAC-R-773. doi:10.2172/877507.
[23] Böhlen TT, Cerutti F, Chin MPW, Fassò A, Ferrari A, Ortega PG, et al. The FLUKA code: developments and challenges for high energy and medical applications. Nucl Data Sheets 2014;120:211–4. https://doi.org/10.1016/j.nds.2014.07.049.
[24] Özkalaycı F, Kaçal MR, Agar O, Polat H, Sharma A, Akman F. Lead(II) chloride effects on nuclear shielding capabilities of polymer composites. J Phys Chem Solids 2020;145:109543. https://doi.org/10.1016/j.jpcs.2020.109543.
[25] Rashad M, Rüsing M, Berth G, Lischka K, Pawlis A. CuO and Co3 O4 nanoparticles: synthesis, characterizations, and Raman spectroscopy. J Nanomater 2013;2013:1–6. https://doi.org/10.1155/2013/714853.
[26] JCPDS cards, No. 47-1049 n.d.
[27] Klug LA. X-ray diffraction procedures. New York: Wiley; 1962.
[28] Luitel HN, Mizuno S, Tani T, Takeda Y. Broadband-sensitive Ni 2+ –Er 3+ based upconverters for crystalline silicon solar cells. RSC Adv 2016;6:55499–506. https://doi.org/10.1039/C6RA10713C.
[29] Singh J, Verma NK. Structural, optical and magnetic properties of cobalt-doped CdSe nanoparticles. Bull Mater Sci 2014;37:541–7. https://doi.org/10.1007/s12034-014-0671-4.
[30] Issa SAM, Darwish AAA, El-Nahass MM. The evolution of gamma-rays sensing properties of pure and doped phthalocyanine. Prog Nucl Energy 2017;100:276–82. https://doi.org/10.1016/j.pnucene.2017.06.016.
[31] Issa SAM, Tekin HO. The multiple characterization of gamma, neutron and proton shielding performances of xPbO-(99–x)B2O3–Sm2O3 glass system. Ceram Int 2019;45:23561–71. https://doi.org/10.1016/j.ceramint.2019.08.065.
[32] El-Khayatt AM, Saudy HA. Preparation and characterization of zinc, lanthanum white sand glass for use in nuclear applications. Radiat Phys Chem 2020;166:108497. https://doi.org/10.1016/j.radphyschem.2019.108497.
[33] Kaçal MR, Akman F, Sayyed MI, Akman F. Evaluation of gamma-ray and neutron attenuation properties of some polymers. Nucl Eng Technol 2019;51:818–24. https://doi.org/10.1016/j.net.2018.11.011.
[34] Tekin HO, Kassab LRP, Kilicoglu O, Magalhães ES, Issa SAM, da Silva Mattos GR. Newly developed tellurium oxide glasses for nuclear shielding applications: an extended investigation. J Non Cryst Solids 2019. https://doi.org/10.1016/j.jnoncrysol.2019.119763.
[35] Saudi Heba, Hassan Y, Tarek E, Borham E, Bendary A. Development of advanced, transparent radiation shielding glass possessing boron and lead ions in the glassy matrix. Egypt J Phys 2020:0–0. doi:10.21608/ejphysics.2020.23900.1035.
[36] Abouhaswa AS, Zakaly HMH, Issa SAM, Pyshkina M, El-Mallawany R, Mostafa MYA. Lead borate glasses and synergistic impact of lanthanum oxide additive: optical and nuclear radiation shielding behaviors. J Mater Sci Mater Electron 2020. https://doi.org/10.1007/s10854-020-04009-y.
[37] Tekin HO, Issa SAM, Kavaz E, Altunsoy Guclu EE. The direct effect of Er 2 O 3 on bismuth barium telluro borate glasses for nuclear security applications. Mater Res Express 2019;6:115212. https://doi.org/10.1088/2053-1591/ab4cb5.
[38] Chandra Babu Naidu K, RoopasKiran S, Madhuri W. Investigations on transport, impedance and electromagnetic interference shielding properties of microwave processed NiMg ferrites. Mater Res Bull 2017;(89):125–38. https://doi.org/10.1016/j.materresbull.2017.01.015.
[39] Chandra Babu Naidu K, Madhuri W. Microwave processed bulk and nano NiMg ferrites: a comparative study on X-band electromagnetic interference shielding properties. Mater Chem Phys 2017;187:164–76. https://doi.org/10.1016/j.matchemphys.2016.11.062.